Refining the stable isotope budget for Antarctic Bottom Water: New foraminiferal data from the abyssal southwest Atlantic

J. L. Hoffman[1] and D. C. Lund[1]

Received 29 August 2011; revised 30 December 2011; accepted 9 January 2012; published 29 March 2012.

[1] Stable isotope tracer budget results suggest the transport to vertical diffusivity ratio for Antarctic Bottom Water (AABW) in the Atlantic was higher at the Last Glacial Maximum (LGM). Reduced mixing across the upper boundary of AABW is consistent with movement of this surface away from the seafloor and may be a factor in sequestering CO_2 in the abyssal Atlantic. Two key unknowns in the budget are the isotopic composition of AABW and the spatial representativeness of isolated vertical profiles of $\delta^{18}O$ and $\delta^{13}C$. Due to a lack of core material below 3 km water depth, Lund et al. (2011) based their Holocene budget on water column data and their LGM budget on extrapolation of isotopic trends from shallower cores. Here we determine $\delta^{18}O$ and $\delta^{13}C$ for AABW using new isotopic records from 3 to 4 km water depth at the Brazil Margin. The core top data yield tracer budget parameters consistent with water column data in the broader Southwest Atlantic. At the LGM, benthic $\delta^{18}O$ reaches 4.9‰ at 4 km water depth, the highest LGM $\delta^{18}O$ value in the published literature. The corresponding $\delta^{13}C$ of −0.2‰ is less depleted than expected and >0.5‰ greater than $\delta^{13}C$ in the Southeast Atlantic. Our Peclet number estimates suggest $\delta^{13}C$ acted conservatively during both the Holocene and LGM. Both $\delta^{18}O$ and $\delta^{13}C$ imply the transport to vertical diffusivity ratio for AABW was an order of magnitude larger during the LGM, due to enhanced AABW transport or reduced mixing across its upper boundary.

Citation: Hoffman, J. L., and D. C. Lund (2012), Refining the stable isotope budget for Antarctic Bottom Water: New foraminiferal data from the abyssal southwest Atlantic, *Paleoceanography*, *27*, PA1213, doi:10.1029/2011PA002216.

1. Introduction

[2] The distribution of $\delta^{13}C$ in the western Atlantic was very different during the Last Glacial Maximum (LGM) than today. Today, ^{13}C-depleted Antarctic Bottom Water (AABW) exists primarily south of the equator and at depths below 3000 m. The vertical $\delta^{13}C$ gradient across the upper boundary of AABW is less than 0.5‰ [*Kroopnick*, 1985]. By comparison, the glacial Atlantic contained low $\delta^{13}C$ AABW that filled the basin from the bottom to 2 km water depth and from the Southern Ocean to approximately 50°N [*Curry and Lohmann*, 1982; *Curry and Oppo*, 2005; *Duplessy et al.*, 1988]. In the southwest Atlantic, the $\delta^{13}C$ of AABW contrasted with overlying water by as much as 1‰ [*Curry and Oppo*, 2005]. In the southeast Atlantic, the contrast approached 1.5‰ [*Ninnemann and Charles*, 2002].

[3] Reconstructions of the glacial deep Atlantic water mass distribution have been based primarily on benthic foraminiferal $\delta^{13}C$. However, remineralization of organic carbon may mask the effect of oceanic circulation and mixing on the $\delta^{13}C$ tracer field. The tracer budget developed by *Lund et al.* [2011] instead relies on benthic foraminiferal $\delta^{18}O$ as a water mass tracer because it is dependent on the conservative properties of temperature and seawater $\delta^{18}O$. Unlike $\delta^{13}C$, foraminiferal $\delta^{18}O$ in the ocean interior changes primarily due to mixing with water masses of different $\delta^{18}O$ values. A key finding of *Lund et al.* [2011] was that the LGM ratio of AABW transport to vertical mixing across the upper boundary of AABW was at least twice what it is today. Thus, greater isotopic stratification in the glacial Atlantic was driven by either enhanced AABW transport or reduced vertical mixing.

[4] In this paper, we address two important gaps in our knowledge of the tracer parameters for AABW. The Holocene tracer budget by *Lund et al.* [2011] was based on water column data because foraminifera were not available from the depth range where AABW flows into the South Atlantic. This precluded a test of whether tracer parameters based on core top foraminifera from the Brazil Margin are representative of the broader Atlantic. Furthermore, the lack of deep core material required that the LGM $\delta^{18}O$ and $\delta^{13}C$ values for AABW be based on extrapolation of isotopic trends shallower in the water column. Here we constrain $\delta^{18}O$ and $\delta^{13}C$ for AABW in the South Atlantic for both the Holocene and LGM using a new set of cores from 3 to 4 km water depth. We also present radiocarbon dates that allow us to create a common chronologic framework for the tracer

[1]Department of Earth and Environmental Sciences, University of Michigan, Ann Arbor, Michigan, USA.

Copyright 2012 by the American Geophysical Union.
0883-8305/12/2011PA002216

Table 1. Depth, Names, Locations, and Stable Isotope Results for the Cores Used in This Study[a]

Water Depth (m)	Core	Location	Holocene (5–7 kyr BP) δ^{13}C (‰ VPDB)	Holocene (5–7 kyr BP) δ^{18}O (‰ VPDB)	*Curry and Oppo* [2005] Core Top δ^{18}O (‰ VPDB)	LGM (19–26 kyr BP) δ^{13}C (‰ VPDB)	LGM (19–26 kyr BP) δ^{18}O (‰ VPDB)	LGM (Highest δ^{18}O) δ^{18}O (‰ VPDB)
1268	36GGC	27°15′S, 46°28′W	*0.91 ± 0.22*	*2.52 ± 0.06*	*2.53 ± 0.09*	*0.60 ± 0.07*	*4.15 ± 0.10*	*4.20 ± 0.06*
1627	17JPC	27°42′S, 46°30′W	0.96 ± 0.13*	2.60 ± 0.15*	2.84 ± 0.10*	n/a	n/a	4.30 ± 0.17
2082	33GGC	27°33′S, 46°05′W	1.18 ± 0.09*	2.55 ± 0.07*	2.37 ± 0.10*	n/a	n/a	4.55 ± 0.08
2296	42JPC	27°46′S, 46°02′W	*1.28 ± 0.08*	*2.55 ± 0.12*	*2.54 ± 0.09*	*0.55 ± 0.08*	*4.53 ± 0.10*	*4.61 ± 0.04*
3353	120GGC	28°35′S, 45°14′W	0.84 ± 0.08*	2.98 ± 0.14*	n/a	n/a	n/a	4.72 ± 0.06*
3589	125GGC	29°32′S, 45°05′W	0.68 ± 0.07	3.16 ± 0.15	n/a	0.13 ± 0.09	4.74 ± 0.11	4.80 ± 0.07
3924	22GGC	29°47′S, 43°35′W	0.42 ± 0.36	3.12 ± 0.20	n/a	−0.31 ± 0.23	4.85 ± 0.15	4.87 ± 0.24
4003	54GGC	29°32′S, 43°20′W	0.36 ± 0.43	3.31 ± 0.14	n/a	−0.05 ± 0.13	4.85 ± 0.05	4.88 ± 0.06

[a]Mean and one-sigma uncertainties are given for the Holocene (5–7 kyr BP), core top, LGM (19–26 kyr BP), and LGM (highest δ^{18}O values). Stable isotopic results from *Curry and Oppo* [2005] are shown in italics. Asterisks denote values where age control is based on oxygen isotope stratigraphy.

profiles. As a result, we are able to avoid potential problems in using δ^{18}O as both a circulation tracer and stratigraphic tool.

2. Methods

[5] The cores used in this study were retrieved during the KNR159–5 cruise along the Brazil Margin in the South Atlantic [*Curry and Oppo*, 2005]. The cores range in water depth from 1200 to 4000 m, including 36GGC, 17JPC, 33GGC, 42JPC, 120GGC, 125GGC, 22GGC, and 54GGC (Table 1). Samples were collected at 4 or 5 cm intervals, freeze-dried, and washed through a 63 μm sieve. Each sample was picked for benthic foraminifera (*Cibicidoides spp)* from the >250 μm size fraction. We then analyzed the foraminifera individually for δ^{18}O and δ^{13}C using standard procedures [*Ostermann and Curry*, 2000]. Our samples were run on a triple-collector gas source mass spectrometer coupled to a Finnigan Kiel automated preparation device at the Stable Isotope Laboratory at the University of Michigan. Data were converted to Vienna Pee Dee Belemnite (VPDB) using NBS 19 (n = 78, δ^{13}C = 1.93 ± 0.04, δ^{18}O = −2.20 ± 0.07‰) and NBS 18 (n = 28, δ^{13}C = −5.03 ± 0.06, δ^{18}O = −22.98 ± 0.07‰).

2.1. Inter-Laboratory Calibration

[6] *Ostermann and Curry* [2000] showed that measurements of δ^{18}O standards can vary by up to 0.3‰ between different laboratories. Similar offsets have been observed between laboratories running benthic foraminifera from the same sediment core [*Hodell et al.*, 2003]. Although this level of uncertainty is acceptable for the purpose of developing an isotopic stratigraphy, it is problematic for the δ^{18}O tracer budget because the spatial variability of δ^{18}O in the deep Atlantic, during both the Holocene and LGM, is less than 0.5‰ [*Lund et al.*, 2011].

[7] Integration of stable isotope data from multiple laboratories requires careful monitoring using not only NBS19 (δ^{18}O = −2.20‰) but also a well-constrained standard on the 'heavy' end of the oxygen isotopic scale. To evaluate the fidelity of the δ^{18}O values in our cores, we used the Atlantis II standard (δ^{18}O = 3.42‰) [*Ostermann and Curry*, 2000]. This standard is more than 5‰ closer in isotopic composition to our LGM δ^{18}O data than NBS19. Atlantis II standards run at the University of Michigan Stable Isotope Laboratory during the course of this study yield a mean δ^{18}O value of 3.45 ± 0.06‰ (n = 90), within one-sigma error of the value established by *Ostermann and Curry* [2000].

[8] As a test of our standard calibration, we compare the δ^{18}O results from core KNR159-5-17JPC run both at the University of Michigan and at Woods Hole Oceanographic Institution (WHOI) (Figure 1). For the LGM (60–90 cm), the Michigan results yield a mean δ^{18}O of 4.30 ± 0.03‰ (±1SE; n = 47) compared to the WHOI mean of 4.19 ± 0.03‰ (±1SE; n = 4) [*Curry and Oppo*, 2005]. Using a Student *t* test and a threshold two-sided *p* value of 0.05, we are unable to reject the null hypothesis that the mean of the WHOI and Michigan samples are the same. For core 33GGC, the mean δ^{18}O for results from Michigan is 4.55 ± 0.03‰ (±1 SE; n = 10), compared to a WHOI-based value of 4.49 ± 0.02‰ (±1 SE; n = 5) (Figure 1, right). As for 17JPC, we cannot reject the null hypothesis that the mean of the WHOI and Michigan samples are the same. Data from the two separate laboratories can therefore be combined to form coherent vertical profiles of δ^{18}O with offsets on par with the typical analytical error for an individual δ^{18}O measurement (±0.1‰).

2.2. Age Models

[9] Our age models are based on radiocarbon dates of planktonic foraminifera (*G. ruber* > 250 μm size fraction). The weights of *G. ruber* samples used for ^{14}C analysis ranged between 1 and 5 mg. In cases where the total mass of *G. ruber* individuals was less than 1 mg, we supplemented the sample with tests of *G. sacculifer*. Samples were prepared for ^{14}C analysis following standard procedures at the Keck Carbon Cycle Accelerated Mass Spectrometer Laboratory at the University of California Irvine. For surface water reservoir ages, we used a ΔR of zero with a one-sigma error of ±200 years. The modern surface water reservoir at 27°S on the Brazil Margin is 407 ± 59 years and the ΔR is 7 ± 59 (n = 12) [*Angulo et al.*, 2007]. We used a ΔR error of ±200 years to account for unknown changes in reservoir age during the last 25,000 years. Calendar ages were calibrated using *Calib* v.6.0 (http://calib.qub.ac.uk/calib/).

2.3. Tracer Budgets

[10] In this section, we discuss the updated methods we used for calculating tracer budget parameters and an abbreviated summary of the δ^{18}O and δ^{13}C budget equations. A full description of the methodology is given by *Lund et al.* [2011].

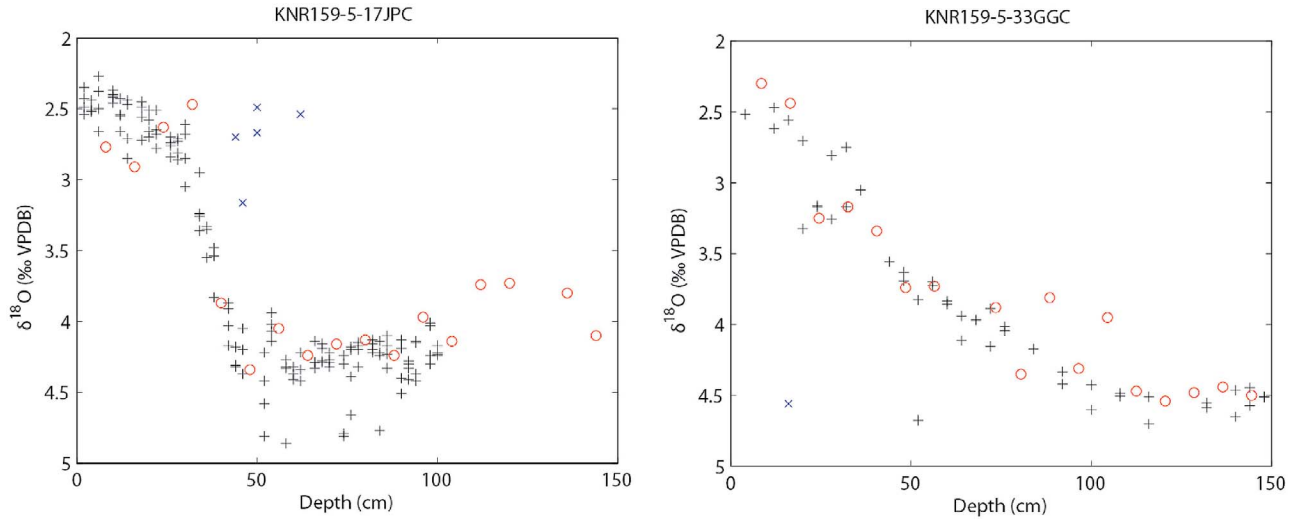

Figure 1. Benthic foraminiferal $\delta^{18}O$ results for (left) KNR159-5-17JPC and (right) KNR159-5-33GGC plotted versus depth in each core. The results from Woods Hole Oceanographic Institution [*Curry and Oppo*, 2005] (red circles) are very similar to those from the University of Michigan (black crosses). Outliers from 40 to 60 cm in 17JPC and at 16.5 cm and 52.5 cm in 33GGC (blue x symbols) are most likely due to burrowing.

2.3.1. The $\delta^{18}O$ Budget

[11] The advection-diffusion balance for $\delta^{18}O$ associated with AABW is described by the following equation:

$$2/3\,\Psi\,\Delta\delta^{18}O \approx \kappa\,\delta^{18}O_z A \tag{1}$$

where the advective flux of $\delta^{18}O$ on the left-hand side of the equation is a function of AABW transport, Ψ ($m^3\ s^{-1}$), and the difference in $\delta^{18}O$ between water near the seafloor and at the upper 'lid' of AABW, $\Delta\delta^{18}O$ (‰). The scaling factor of 2/3 accounts for the fact that the budget domain does not include southward advection. The diffusive flux of $\delta^{18}O$ on the right-hand side of the equation is a function of vertical mixing, κ ($m^2\ s^{-1}$), the vertical gradient in $\delta^{18}O$ at the upper boundary of AABW in the Atlantic, $\delta^{18}O_z$ (‰ m^{-1}), and the area over which mixing occurs, A (m^2). Re-arranging equation (1) such that the measureable quantities are the right-hand side, we obtain:

$$\frac{\Psi}{\kappa} \approx \frac{3}{2}\frac{\delta^{18}O_z}{\Delta\delta^{18}O}A \tag{2}$$

where the ratio of advection to vertical mixing (Ψ/κ) for AABW is a function of $\delta^{18}O_z$, $\Delta\delta^{18}O$, and A. The domain for the $\delta^{18}O$ budget encompasses a volume of water below a constant tracer surface and north of 30°S (the approximate latitude of the Brazil Margin cores). The tracer surface that defines the upper boundary of AABW corresponds to the $\delta^{18}O$ value where the vertical gradient in $\delta^{18}O$ ($\delta^{18}O_z$) is largest. In the modern Southwest Atlantic, the maximum $\delta^{18}O_z$ estimated from water column data is closely associated with the upper boundary of AABW [*Lund et al.*, 2011].

[12] We determined the upper boundary of AABW during the Holocene and LGM using the vertical profile of foraminiferal $\delta^{18}O$ for each time interval. We assigned a calibration error of ± 0.18‰ (1σ) to the mean $\delta^{18}O$ value at each water depth [*Marchal and Curry*, 2008]. Using these statistical constraints, we then generated 1000 random vertical profiles of $\delta^{18}O$ using a Monte Carlo approach. Unlike in the work by *Lund et al.* [2011], each $\delta^{18}O$ profile was sampled at 200 m increments (the average depth spacing for the cores at Brazil Margin) to calculate $\delta^{18}O_z$. We did this to eliminate bias in the $\delta^{18}O_z$ estimates that results from data points spaced closely together in water depth.

[13] The new foraminiferal data below 3 km water depth allow for direct determination of the isotopic composition of AABW as it enters the South Atlantic. We use stable isotopic results at 3.9 km (22GGC) and 4.0 km (54GGC) to represent AABW during the Holocene and LGM. We subtract $\delta^{18}O$ at 3.9–4.0 km from $\delta^{18}O$ at the upper boundary of AABW to estimate $\Delta\delta^{18}O$. Thus we now calculate $\Delta\delta^{18}O$ in exactly the same way for the Holocene and LGM.

[14] Because foraminifera record in situ rather than potential temperature, we correct the Holocene and LGM $\Delta\delta^{18}O$ values for the effect of compressive heating. In the case of the modern AABW, hydrostatic pressure makes water at 4 km water depth about 0.1°C warmer than water at 3 km. Given a $\delta^{18}O$-T relationship of 0.2 ‰ per °C, the $\delta^{18}O$ value at 4 km is reduced by about 0.02‰. We therefore add 0.02‰ to our Holocene foraminiferal $\Delta\delta^{18}O$ estimate to compensate for this effect. During the LGM, the correction is larger (0.05‰) because the upper boundary of AABW was near 2000 m water depth. For both time intervals, this correction yields modest (5–10%) reductions in Ψ/κ.

2.3.2. The $\delta^{13}C$ Budget

[15] The $\delta^{13}C$ of dissolved inorganic carbon is sensitive to not only transport and mixing but also biological remineralization. As a result, the tracer budget for $\delta^{13}C$ includes a remineralization term, J (‰ s^{-1}), multiplied by the volume into which the remineralization occurs, V (m^3):

$$2/3\,\Psi\,\Delta\delta^{13}C + JV \approx \kappa\,\delta^{13}C_z A \tag{3}$$

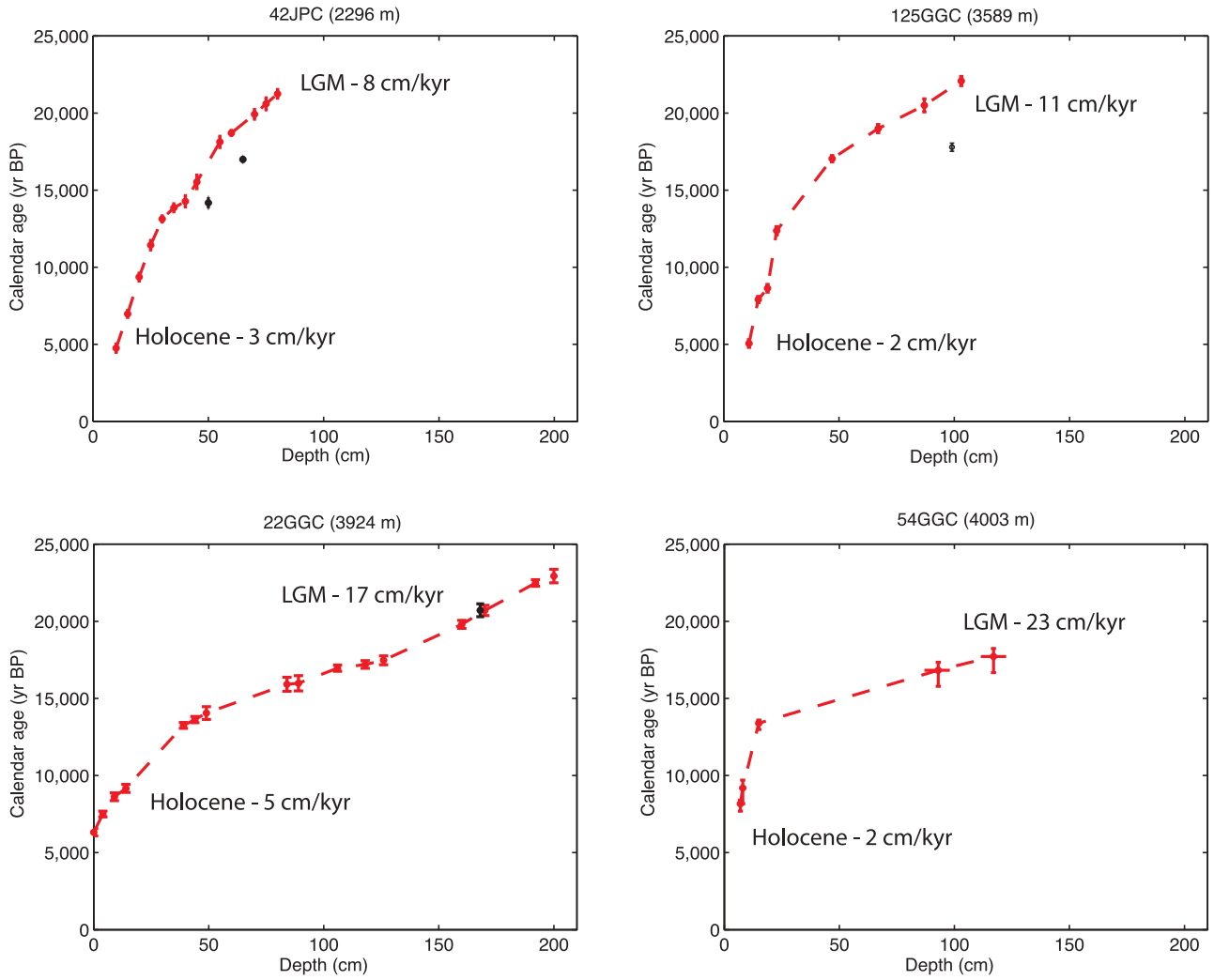

Figure 2. Calendar ages (red circles) and age models (dashed lines) for cores 42JPC, 125GGC, 22GGC, and 54GGC. Error bars for each calendar age represent the $\pm 1\sigma$ uncertainty. Age reversals not included in each age model are shown as black symbols. Due to low benthic foraminiferal abundance, the two deepest ages in 54GGC each span 10 cm intervals (horizontal red lines). All cores have higher sedimentation rates during the LGM and deglaciation than the Holocene. Note that the core top age for both 125GGC and 22GGC is ~5 kyr BP. The core tope age for 54GGC is ~7 kyr BP.

where $\delta^{13}C_z$ is the gradient in $\delta^{13}C$ at the upper boundary of AABW and $\Delta\delta^{13}C$ is the difference in $\delta^{13}C$ between water entering the South Atlantic and $\delta^{13}C$ at the AABW 'lid'. For $\delta^{13}C$, the diffusive flux ($\kappa\ \delta^{13}C_z\ A$) is balanced by the advective flux (2/3 $\Psi\ \Delta\delta^{13}C$) plus the remineralization flux (JV). Dividing through by the diffusive flux and re-arranging terms, we obtain:

$$Pe = \frac{2}{3}\frac{\Psi}{\kappa}\frac{\Delta\delta^{13}C}{\delta^{13}C_z A} = \frac{\delta^{18}O_z}{\Delta\delta^{18}O}\frac{\Delta\delta^{13}C}{\delta^{13}C_z} \quad (4)$$

where the first term is a bulk Peclet number, *Pe*, the non-dimensional ratio of tracer transport to tracer diffusion. Through substitution with equation (2), the area terms cancel and we see that *Pe* can be determined using the tracer parameters $\delta^{18}O_z$, $\Delta\delta^{18}O$, $\delta^{13}C_z$, and $\Delta\delta^{13}C$.

[16] We estimated $\delta^{13}C_z$ for the upper boundary of AABW in the same way as $\delta^{18}O_z$ but we instead use a calibration error of ± 0.14‰ (1σ) for each $\delta^{13}C$ value [*Lund et al.*, 2011]. In certain cases the uncertainty in mean $\delta^{13}C$ values from individual cores exceeds ± 0.14‰. In these instances, we use the $\pm 1\sigma$ uncertainty from the raw data. For the Holocene, we use one-sigma uncertainties of ± 0.4‰ for the cores at 3.9 and 4.0 km water depth (Table 1). For the LGM, we use one-sigma uncertainties of ± 0.3‰ for the cores at 1.6, 3.3, and 3.9 km water depth. We calculate $\Delta\delta^{13}C$ by subtracting the $\delta^{13}C$ value where $\delta^{13}C_z$ is greatest from $\delta^{13}C$ at 3900–4000 m. The net outcome of our analysis of the stable isotope profiles is 1000 estimates of $\delta^{18}O_z$, $\Delta\delta^{18}O$, $\delta^{13}C_z$, and $\Delta\delta^{13}C$ for both the Holocene and LGM.

3. Results and Discussion

3.1. Age Models

[17] Age models for the KNR159–5 cores are shown in Figure 2, including 42JPC, 125GGC, 22GGC, and 54GGC.

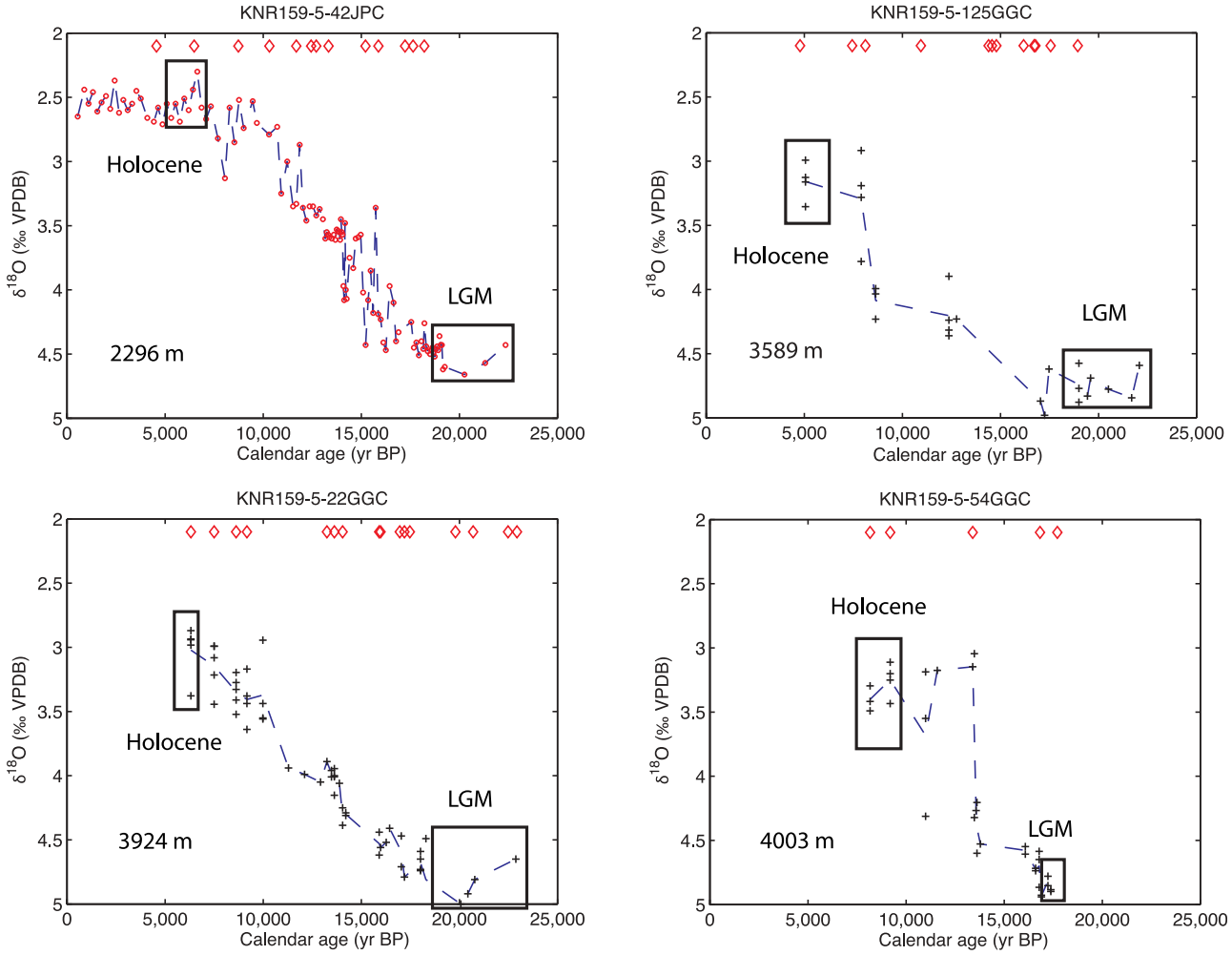

Figure 3. Radiocarbon-constrained δ^{18}O time series for the Brazil Margin. Boxes indicate intervals used for calculating mean Holocene and LGM values. Each point represents the δ^{18}O result for an individual foraminifer. Red circles are data from *Curry and Oppo* [2005] and black crosses are from this study. Dashed line indicates average the value for each stratigraphic level in the core. Diamonds denote calendar ages for each core. The highest LGM δ^{18}O values occur at the deepest sites, reaching a maximum of 4.9‰ at 4000 m water depth.

The age model for 36GGC is presented by *Sortor and Lund* [2011]. As expected, each core generally exhibits increasing ages with depth. Sedimentation rates are highest during the LGM and deglaciation and then decrease during the Holocene. Overall, sedimentation rates during the LGM and deglaciation range from 8 to 23 cm/kyr while Holocene rates range from 2 to 5 cm/kyr. The highest sedimentation rates occur at the deepest sites, most likely due to localized sediment drifts. Age reversals on the order of hundreds to thousands of years occur in the Brazil Margin cores. In the case of 36GGC, the age reversals are most likely due to burrowing of material from up section [*Sortor and Lund*, 2011]. We assume that a similar process accounts for the 1–2 kyr reversals in 42JPC and 125GGC and we therefore exclude these ages.

[18] In the case of 125GGC, 22GGC, and 54GGC, the core top material is mid-Holocene in age (Figure 3). This could be due to an artifact of the coring process, slowing of sedimentation rates during the late Holocene, or erosion by deep currents. Based on the available data we cannot distinguish between these three possibilities. Because the cores lack material for the late Holocene, we base our stable isotope profiles on the time interval from 5 to 7 kyr BP. We chose this interval because it is the youngest material that exists in all of the cores at the Brazil Margin. The one exception is core 54GGC, where the Holocene values range in age from 7 to 9 kyr BP.

3.2. Sensitivity of Isotopic Results to Age Interval Choice

[19] Given that we integrate our stable isotope results with those from *Curry and Oppo* [2005] it is necessary to ensure that their core top data are similar to our mid-Holocene results. We test this by comparing the core top and 5–7 kyr BP data from cores run by *Curry and Oppo* [2005] where we have acquired radiocarbon dates (cores 36GGC and 42JPC). We find that there is no significant difference in mean stable isotopic values between the core tops and 5–7 kyr BP

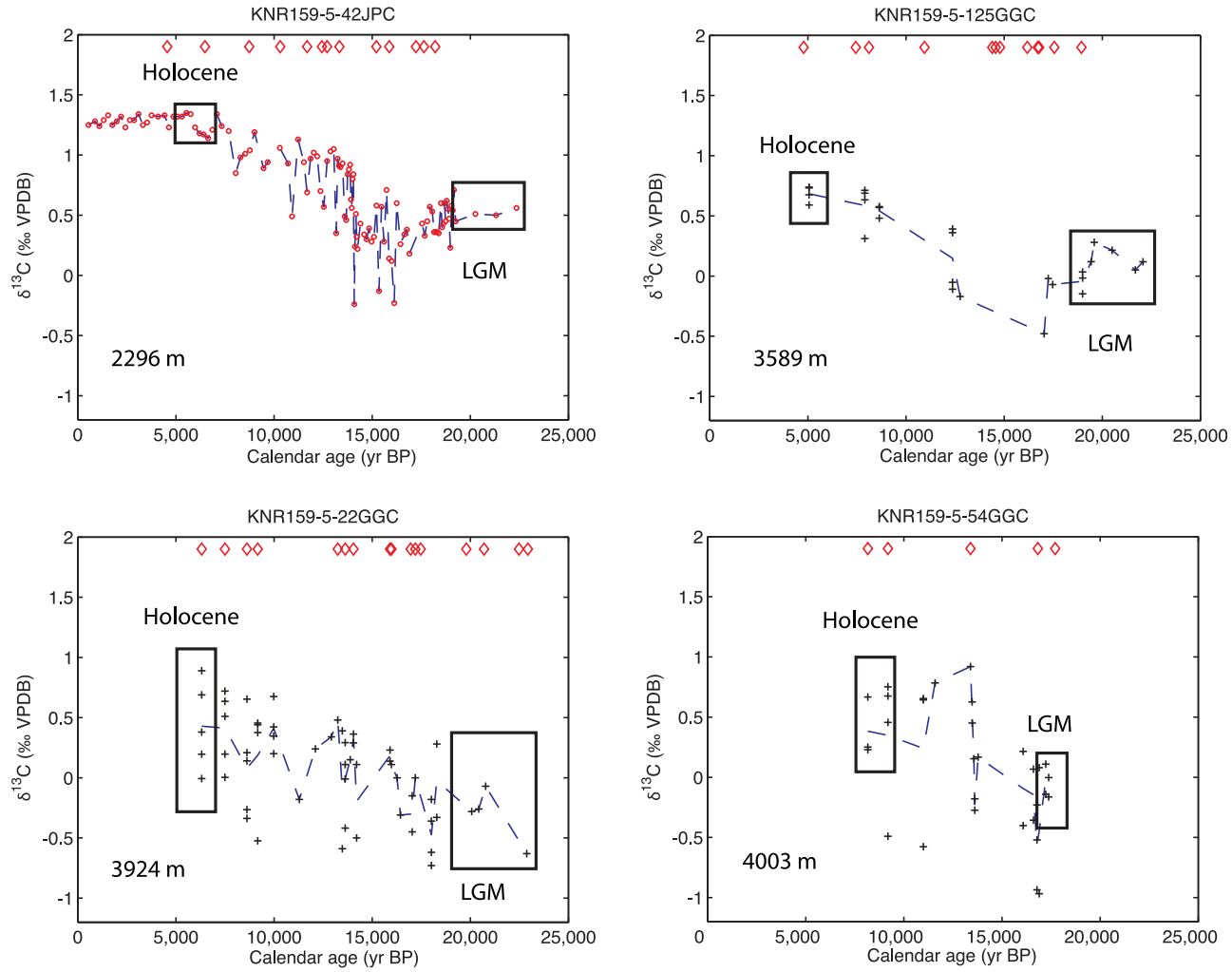

Figure 4. Radiocarbon-constrained δ^{13}C time series for the Brazil Margin. Boxes indicate intervals used for calculating mean Holocene and LGM values. Each point represents the δ^{13}C value for an individual foraminifer. Red circles are stable isotope data from *Curry and Oppo* [2005] and black crosses are new results from this study. Diamonds at the top of each plot indicate calendar ages for each core. The δ^{13}C values generally increase from the LGM into the Holocene, but in some cases the time series exhibit negative excursions during the deglaciation (e.g., 42JPC, 125GGC).

(Table 1). This result is not surprising given the nearly constant stable isotopic time series for 42JPC from the mid- to late-Holocene (Figures 3 and 4). Similarly, data from core 17JPC run at the University of Michigan shows little change in stable isotopic values during the Holocene (Figure 1). Coherent vertical profiles of δ^{18}O and δ^{13}C can therefore be constructed using material that spans the Holocene in the Brazil Margin cores.

[20] Another important age model-related issue concerns the definition of the LGM. In the work by *Curry and Oppo* [2005], the LGM was classically defined as the interval with the highest δ^{18}O values in the time series. Because we are using δ^{18}O as a water mass tracer and subtle changes in the vertical δ^{18}O profile are important for the tracer budget, it is preferable to define the LGM using independent chronologic constraints. Here we use the calendar-calibrated radiocarbon ages for each core to define the LGM interval (19–26 kyr BP) [*Clark et al.*, 2009]. We find that the two definitions of the LGM yield very similar mean LGM stable isotope values (Table 1). For example, the mean LGM δ^{18}O for 42JPC based on the 19–26 kyr BP definition is 4.53 $\pm$ 0.04‰ compared to the *Curry and Oppo* [2005] value of 4.61 $\pm$ 0.04‰. We can therefore combine LGM data from *Curry and Oppo* [2005] that have no radiocarbon constraints with the LGM picks presented in this paper to create a single δ^{18}O profile.

[21] Results for core KNR159-5-120GGC are shown in Figure 5. This core lacks radiocarbon dates and the δ^{18}O and δ^{13}C time series are sparse compared to the other cores presented in this paper. Nonetheless, the mean Holocene and LGM δ^{18}O and δ^{13}C for 120GGC are consistent with values from adjacent water depths (Table 1 and Figures 6 and 8).

3.3. Vertical Profiles of δ^{18}O

[22] Using our δ^{18}O picks we plot vertical profiles of δ^{18}O for the Holocene and LGM in Figure 6. Mid-Holocene δ^{18}O for the deeper cores range from 2.5‰ to 3.3‰ with the most positive values occurring at the greatest water depths. The

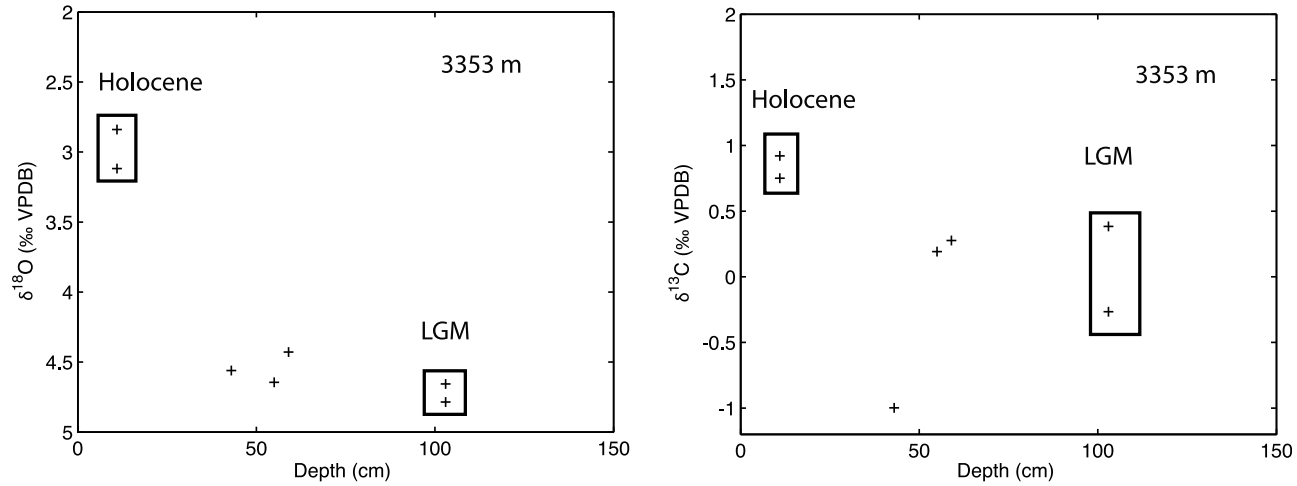

Figure 5. The (left) $\delta^{18}O$ and (right) $\delta^{13}C$ results for core KNR159-5-120GGC, which lacked adequate planktonic foraminifera to obtain reliable radiocarbon ages. The mean LGM results were calculated using the most positive $\delta^{18}O$ results in each core. As for the other cores, 120GGC exhibits the expected patterns of high $\delta^{18}O$ values during the LGM and low $\delta^{18}O$ during the Holocene.

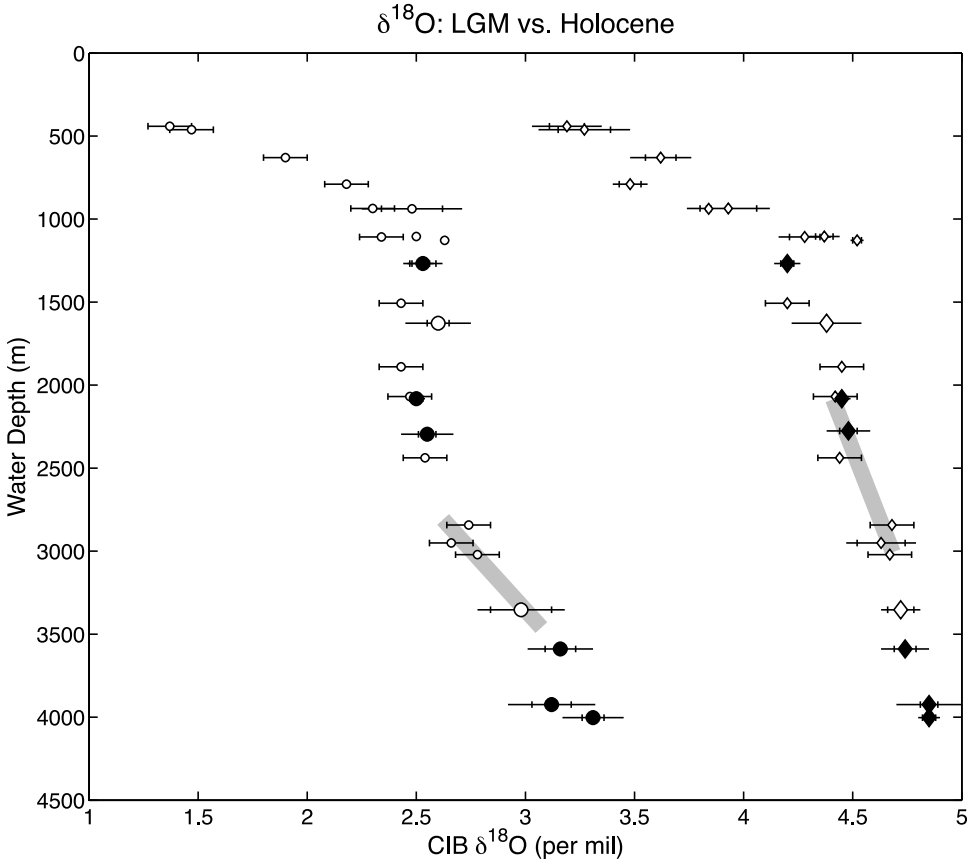

Figure 6. Vertical profiles of $\delta^{18}O$ for the Holocene (circles) and LGM (diamonds). Large markers are based on data from this paper and small markers are based on data from *Curry and Oppo* [2005]. Open symbols indicate data not constrained by radiocarbon dates. Horizontal lines represent one-sigma uncertainties while vertical hash marks are the standard error on the mean $\delta^{18}O$ at each water depth. For those points based on one analysis, the one-sigma uncertainty and the standard error are the same. In certain cases, the standard error is smaller than the symbol used to represent the mean. The approximate locations of the water mass boundaries for each time interval (gray bars) are inferred from the two-dimensional histograms in Figure 7.

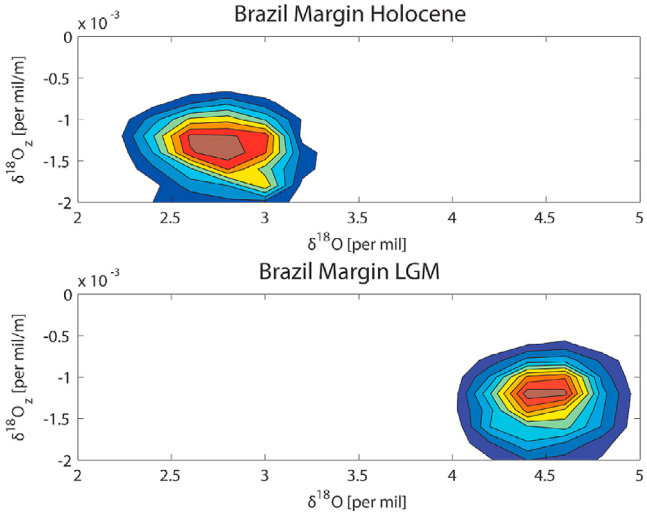

Figure 7. Two-dimensional histograms of foraminiferal $\delta^{18}O_z$ versus $\delta^{18}O$ for the (top) Holocene and (bottom) LGM. The maximum vertical gradient in $\delta^{18}O$ ($\delta^{18}O_z$) occurs at 2.8 ± 0.2‰ during the Holocene and 4.5 ± 0.2‰ during the LGM.

mean $\delta^{18}O$ for the cores at 3.6 km, 3.9 km, and 4.0 km water depth is 3.16 ± 0.15‰. If we exclude the isotopically light value at 3900 m, the mean becomes 3.24 ± 0.11‰. In either case, the Holocene foraminiferal $\delta^{18}O$ value is indistinguishable from estimates based on local hydrographic data at these water depths (3.1–3.2‰) [*Lund et al.*, 2011]. This agreement indicates that benthic foraminifera at the Brazil Margin faithfully record the equilibrium $\delta^{18}O$ value of AABW as it enters the Southwest Atlantic. The maximum vertical gradient in $\delta^{18}O$ ($\delta^{18}O_z$) occurs at a $\delta^{18}O$ value of 2.8 ± 0.2‰ (Figure 7), equivalent to a water depth range of 3000 to 3500 m (Figure 6). This depth is similar to that determined using modern hydrographic data [*Lund et al.*, 2011] and shows that the $\delta^{18}O$ of benthic foraminifera at the Brazil Margin is also a reliable recorder of the upper boundary of AABW.

[23] During the LGM, the vertical profile of $\delta^{18}O$ increases monotonically with water depth to a maximum of 4.85 ± 0.15‰ at 3.9 km and 4.85 ± 0.05‰ at 4.0 km (Figure 6). These are the highest $\delta^{18}O$ values for the South Atlantic in the published literature. Given their magnitude, the geographic proximity of the core sites to the Southern Ocean, and that the flow AABW is focused along the deep western boundary, we believe they are very close to the end-member $\delta^{18}O$ value for AABW during the LGM.

[24] The maximum $\delta^{18}O_z$ in the LGM profile occurs at a $\delta^{18}O$ of 4.5 ± 0.1‰ (Figure 7) equivalent to a water depth range of 2–3 km (Figure 6). The $\delta^{18}O$-derived water mass boundary is deeper than the 1.6 to 2.2 km range determined by *Lund et al.* [2011]. The key difference is that the new data below 3.0 km water depth have a relatively low vertical $\delta^{18}O$ gradient (Figure 6). As a result, the randomly generated $\delta^{18}O$ profiles tend to have maximum $\delta^{18}O_z$ values between 2 and 3 km. This finding pushes the $\delta^{18}O$-based water mass boundary for AABW deeper in the water column making it more consistent with the depth range inferred from the LGM $\delta^{13}C$ profile.

3.4. Vertical Profiles of $\delta^{13}C$

[25] Using our $\delta^{13}C$ picks we plot vertical profiles of $\delta^{13}C$ for the Holocene and LGM in Figure 8. The $\delta^{13}C$ minimum in the Holocene profile at 1.5 km reflects the presence of upper Circumpolar Deep Water (CDW) while the maximum at 2.5 km is due to the influence of North Atlantic Deep Water [*Curry and Oppo*, 2005]. Low $\delta^{13}C$ values below 3 km are associated with ^{13}C-depleted AABW. The two deepest points at 3.9 and 4.0 km yield an average $\delta^{13}C$ of 0.4 ± 0.2‰ (1σ). This value is within error of water column-based measurements of $\delta^{13}C$ for AABW (0.46 ± 0.02‰) [*Lund et al.*, 2011], further confirming that the deepest Brazil Margin sites monitor AABW as it enters the Southwest Atlantic. The maximum vertical gradient in $\delta^{13}C$ occurs from 3.0 to 3.5 km water depth (Figure 8). Thus, both the $\delta^{18}O$ and $\delta^{13}C$ profiles yield similar depth estimates for the upper 'lid' of AABW during the Holocene.

[26] The shape of the LGM $\delta^{13}C$ profile at the Brazil Margin is similar to the Holocene profile. A $\delta^{13}C$ minimum at 1.2 km documents the presence of southern source intermediate water and a maximum $\delta^{13}C$ at 1.6 km reflects the influence of Glacial North Atlantic Intermediate Water (GNAIW) [*Curry and Oppo*, 2005]. Below 1.6 km $\delta^{13}C$ decreases to −0.31 ± 0.23‰ (1σ) at 3.9 km and −0.05 ± 0.13‰ (1σ) at 4.0 km, yielding an average abyssal value of −0.2 ± 0.2‰. Although a few individual $\delta^{13}C$ results are lower than −0.5‰ in these cores, the vast majority of the data fall between 0‰ and −0.5‰ (Figures 4 and 5). An AABW $\delta^{13}C$ of −0.2‰ is more than 0.5‰ greater than both the AABW $\delta^{13}C$ value used by *Lund et al.* [2011] and LGM $\delta^{13}C$ in the abyssal southeastern Atlantic [*Ninnemann and Charles*, 2002]. The maximum vertical gradient in $\delta^{13}C$ during the LGM occurred over a broad $\delta^{13}C$ range of 0.4 ± 0.2‰ (Figure 9). These $\delta^{13}C_z$ maxima correspond to 2–3 km water depth range (Figure 8), similar to that inferred from $\delta^{18}O$. Thus both tracers yield a similar depth estimate for the upper 'lid' of AABW during the LGM.

[27] It has been suggested that highly depleted ^{13}C values in benthic foraminifera may be due to epibenthic decay of organic matter at the sediment-seawater interface [*Mackensen et al.*, 1993]. We believe this is a secondary effect at the Brazil Margin because both $\delta^{18}O$ and $\delta^{13}C$ show similar trends with water depth. The simplest explanation of these trends is the presence of a water mass both enriched in ^{18}O and depleted in ^{13}C. By comparison, the southeastern Atlantic was apparently occupied by a water mass with lower $\delta^{13}C$ (−0.9 ± 0.1‰) and $\delta^{18}O$ (4.2 ± 0.1‰) [*Ninnemann and Charles*, 2002]. Some of the discrepancy in $\delta^{18}O$ may be due to inter-laboratory calibration, but such issues are unlikely to account for the full 0.7‰ difference. It therefore appears that the abyssal southeastern Atlantic was occupied by a different water mass during the LGM. For the purposes of the tracer budget, we focus on the Brazil Basin where the majority of AABW flows into the Atlantic today [*Speer and Zenk*, 1993].

3.5. The $\delta^{18}O$ Tracer Budget Results

[28] Histograms of $\delta^{18}O_z$, $\Delta\delta^{18}O$, and $\Delta\delta^{18}O/\ \delta^{18}O_z$ for the Holocene are shown in Figure 10 (left). We estimate a $\Delta\delta^{18}O/\ \delta^{18}O_z$ ratio of 385 ± 164 m using the foraminiferal data, compared to the water column-based value of 395 ±

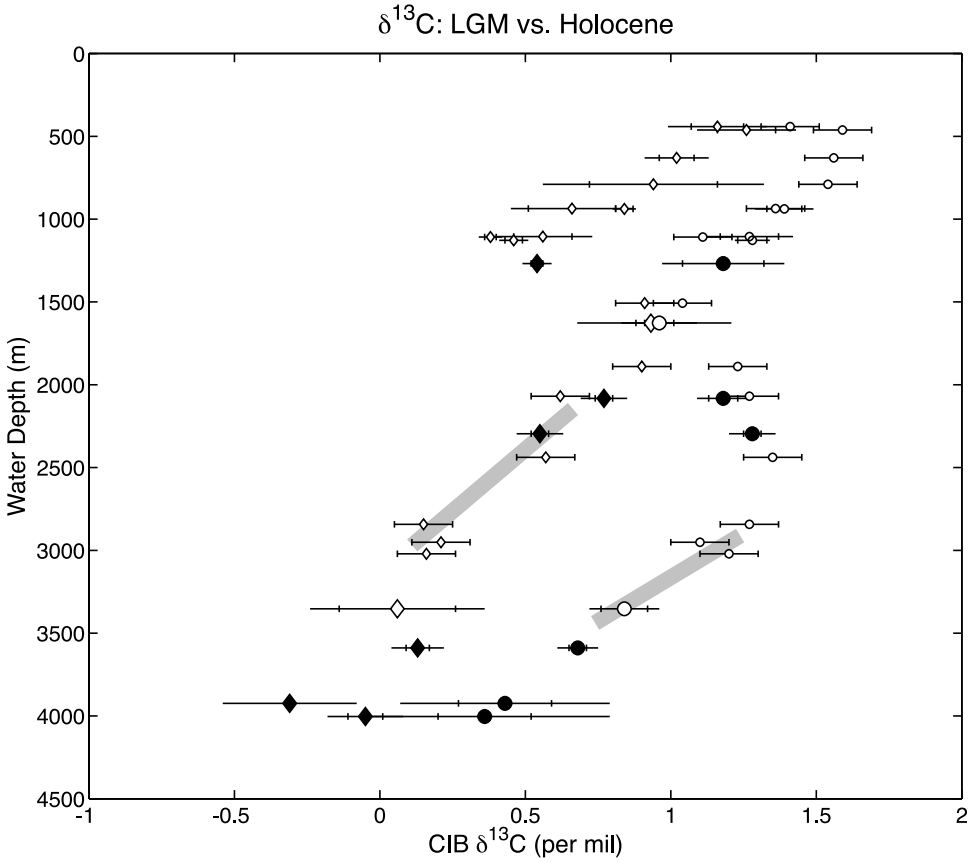

Figure 8. Vertical profiles of $\delta^{13}C$ for the LGM (diamonds) and Holocene (circles). Large markers denote data from this paper, small markers denote data from *Curry and Oppo* [2005], and open symbols indicate cores lacking radiocarbon dates. Horizontal lines represent one-sigma uncertainties while vertical hash marks are the standard error on the mean $\delta^{13}C$ at each depth. For those points based on one analysis, the one-sigma uncertainty and the standard error are the same. In certain cases, the standard error is smaller than the symbol used to represent the mean. The new Holocene below 3000 m extends the $\delta^{13}C$ trend observed shallower in the water column, whereas the new LGM data show little relatively little change in $\delta^{13}C$ below 3500 m. The approximate locations of the water mass boundaries for each time interval (gray bars) are inferred from the two-dimensional histograms in Figure 9.

217 m (Table 2). The latter is based on a hydrographic data spanning the region from approximately 27°S to the equator and 35°W to 20°W [*Lund et al.*, 2011]. The agreement between the foraminiferal and water column-based results indicates that the mid-Holocene profile from the Brazil Margin is an excellent recorder of $\Delta\delta^{18}O/\delta^{18}O_z$ in this region. It also increases our confidence that the Brazil Margin-based estimate of $\Delta\delta^{18}O/\delta^{18}O_z$ at the LGM is representative of the broader Southwest Atlantic. Using the Holocene $\delta^{18}O$ parameters and equation (2), we estimate a Ψ/K for the mid-Holocene of $(1.8 \pm 1.0) \times 10^{10}$ m, which is indistinguishable from the Ψ/K calculated using hydrographic data ($(1.8 \pm 0.8) \times 10^{10}$ m) (Table 2).

[29] With the new cores from 3 to 4 km water depth, we are also able to better constrain AABW during the LGM and therefore more accurately determine $\Delta\delta^{18}O$. We estimate the $\delta^{18}O$ of AABW was approximately 4.9‰ as it entered the Southwest Atlantic (Figure 6). Because the $\delta^{18}O$ at the upper boundary of AABW was approximately 4.5‰ (Figure 7), the median uncorrected $\Delta\delta^{18}O$ was ~0.4‰ (Table 3). We add 0.05‰ to this value to compensate for the effect of compressive heating (see section 2). Based on a $\Delta\delta^{18}O$ of -0.47 ± 0.24‰ and a $\delta^{18}O_z$ of $(-1.3 \pm 0.3) \times 10^{-4}$ ‰ m^{-1}, we estimate an LGM $\Delta\delta^{18}O/\ \delta^{18}O_z$ ratio of 362 ± 206 (Table 3). Multiplying by the area of the 2.5 km isobath in the Atlantic $(4.4 \pm 0.9) \times 10^{13}$ m^2, we estimate a Ψ/K for the LGM of $(1.8 \pm 1.1) \times 10^{11}$ m, slightly higher than the preliminary estimate from *Lund et al.* [2011] ($(1.3 \pm 0.7) \times 10^{11}$ m). Our LGM results are an order of magnitude higher than the Ψ/K estimate for the Holocene. If we use the highest possible LGM $\Delta\delta^{18}O/\ \delta^{18}O_z$ ratio of 900 (Figure 10), the resulting Ψ/K for the LGM is 7.3×10^{10} m. Thus, the minimum Ψ/K for the LGM is at least twice the Holocene value.

3.6. The $\delta^{13}C$ Tracer Budget Results

[30] Histograms of the Holocene $\delta^{13}C_z$, $\Delta\delta^{13}C$, and $\Delta\delta^{13}C/\delta^{13}C_z$ results are shown in Figure 11 (left). Using equation (4) and our estimates of $\Delta\delta^{13}C/\delta^{13}C_z$ and $\Delta\delta^{18}O/\delta^{18}O_z$, we calculate a *Pe* for the Holocene of 0.9 ±

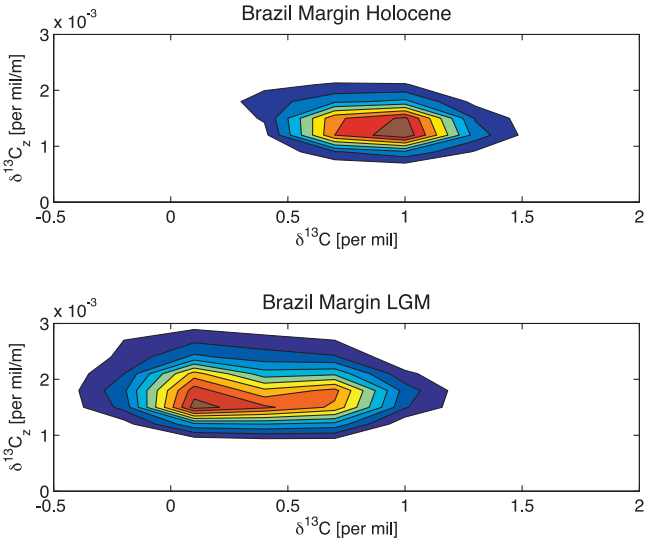

Figure 9. Two-dimensional histograms of $\delta^{13}C_z$ versus $\delta^{13}C$ for (top) Holocene and (bottom) LGM. The maximum vertical gradient in $\delta^{13}C$ ($\delta^{13}C_z$) occurs at a $\delta^{13}C$ value of 1.0 ± 0.3‰ during the Holocene and 0.5 ± 0.3‰ during the LGM.

Table 2. Tracer Budget Parameters for the Holocene[a]

	Water Column Data		Cib Data	
	Mean	Error (±)	Mean	Error (±)
$\delta^{18}O_z$ (‰ m^{-1})	−3.1E-04	8.2E-05	−1.4E-03	3.6E-04
$\Delta\delta^{18}O$* (‰)	−0.12	0.04	−0.55	0.27
$\Delta\delta^{18}O/\delta^{18}O_z$ (m)	385	164	395	217
Area (m^2)	4.7E+12	4.7E+11	4.7E+12	4.7E+11
Ψ/κ (m)	1.8E+10	8.1E+09	1.8E+10	1.0E+10
$\delta^{13}C_z$ (‰ m^{-1})	4.8E−04	9.7E−05	1.4E−03	3.4E−04
$\Delta\delta^{13}C$ (‰)	0.24	0.05	0.48	0.25
$\Delta\delta^{13}C/\delta^{13}C_z$ (m)	514	153	343	197
Area (m^2)	4.7E+12	4.7E+11	4.7E+12	4.7E+11
Ψ/κ (m)	1.4E+10	4.3E+09	2.1E+10	1.2E+10
Pe	1.3	0.7	0.9	0.7

[a]Water column data is for 27°S to 0°N; Cib data is for the Brazil Margin. Asterisk indicates 0.02‰ added to Cib data to adjust for compressional heating.

0.7 (Table 2), consistent with the *Pe* of 1.3 ± 0.7 based on water column data from the Southwest Atlantic [*Lund et al.*, 2011]. Because the *Pe* number is close to 1, it suggests the advective and diffusive fluxes of $\delta^{13}C$ were largely in balance for AABW during the Holocene and that the flux of $\delta^{13}C$ from remineralization played a minor role in setting the $\delta^{13}C$ profile. This is further illustrated by comparing Ψ/κ estimates based on the $\delta^{18}O$ and $\delta^{13}C$ data. If we assume that $\delta^{13}C$ behaves conservatively, $\delta^{13}C_z$ and $\Delta\delta^{13}C$ can be used in place of $\delta^{18}O_z$ and $\Delta\delta^{18}O$ in equation (2). In this case, we estimate a Ψ/κ of (2.1 ± 1.2) × 10^{10} m, indistinguishable from the $\delta^{18}O$-based value of (1.8 ± 1.0) × 10^{10} m (Table 2). Thus, within the error constraints of our budget, it appears that $\delta^{13}C$ behaved conservatively during the Holocene. For this to occur, the residence time for AABW in the

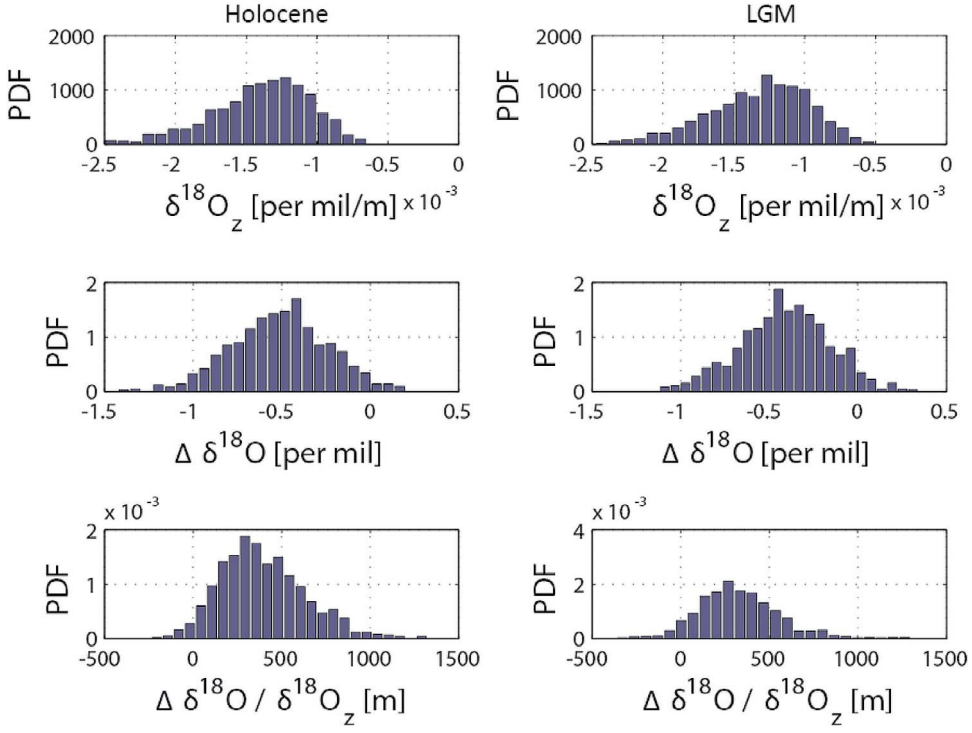

Figure 10. PDFs of $\delta^{18}O_z$, $\Delta\delta^{18}O$, and $\Delta\delta^{18}O/\delta^{18}O_z$ for the (left) Holocene and (right) LGM. The parameter distributions are similar for each time interval. Mean values and uncertainties for each parameter are listed in Tables 2 and 3. We plot $\Delta\delta^{18}O/\delta^{18}O_z$ rather than $\delta^{18}O_z/\Delta\delta^{18}O$ because $\Delta\delta^{18}O$ values close to zero yield infinitely large ratios.

Table 3. Tracer Budget Parameters for the LGM[a]

	Mean	Error (±)
	Cib $\delta^{18}O$ = 4.5	
$\delta^{18}O_z$ (‰ m^{-1})	−1.3E−03	3.3E−04
$\Delta\delta^{18}O$* (‰)	−0.47	0.24
$\Delta\delta^{18}O/\delta^{18}O_z$ (m)	362	206
Area (m^2)	4.4E+13	8.7E+12
Ψ/κ (m)	1.8E+11	1.1E+11
	Cib $\delta^{13}C$ = 0.4	
$\delta^{13}C_z$ (‰ m^{-1})	1.8E−03	4.0E−04
$\Delta\delta^{13}C$ (‰)	0.56	0.32
$\Delta\delta^{13}C/\delta^{13}C_z$ (m)	311	191
Area (m^2)	4.4E+13	8.7E+12
Ψ/κ (m)	2.1E+11	1.4E+11
Pe	0.9	0.7

[a]Area is 2.5 km isobath. Data from Brazil Margin. Asterisk indicates 0.05‰ added to adjust for compressional heating.

Atlantic must be short relative to the amount of time required for remineralization to affect the $\delta^{13}C$ of dissolved inorganic carbon in the abyss.

[31] Histograms of $\delta^{13}C_z$, $\Delta\delta^{13}C$, and $\Delta\delta^{13}C/\delta^{13}C_z$ for the LGM are shown in Figure 11 (right). Overall, the distributions are similar to those for the Holocene, although the mean $\delta^{13}C_z$ for the LGM is somewhat higher. We estimate a *Pe* of 0.9 ± 0.7 for the LGM (Table 3). Given the uncertainty, *Pe* could be less than, equal to, or greater than one. If *Pe* was less than one, the advective flux of $\delta^{13}C$ would be less than the diffusive flux and the remaining flux of ^{13}C-depleted carbon must be supplied by remineralization. On the other hand, if *Pe* was greater than one the tracer budget would be imbalanced and additional flux ^{13}C-enriched carbon would be necessary. One possibility is mixing of GNAIW into AABW along isopycnal surfaces, a flux not included in the tracer budget [*Lund et al.*, 2011].

[32] For the time being, the uncertainty in *Pe* precludes us from quantifying the various fluxes in the LGM $\delta^{13}C$ budget. However, the $\delta^{18}O$- and $\delta^{13}C$-based Ψ/K estimates overlap at one-sigma (Table 3), which suggests $\delta^{13}C$ acted as a largely conservative tracer during the LGM. Advection and diffusion therefore appear to be the primary controls on the tracer profiles. The $\delta^{13}C$-based Ψ/K estimate for the LGM is a factor of ten higher than the Holocene, the same contrast implied by the $\delta^{18}O$ data. Given the different distributions of $\delta^{18}O$ and $\delta^{13}C$ in the LGM Atlantic and the different factors that influence each tracer, the similar Ψ/K estimates strongly suggest the flux of AABW was greater at the LGM or vertical mixing across the upper 'lid' of AABW was reduced compared to today.

3.7. Future Work

[33] Given the monotonic increase in $\delta^{13}C$ from the LGM to Holocene in other deep Atlantic cores [e.g., *Ninnemann and Charles*, 2002], we expected $\delta^{13}C$ time series at the Brazil Margin to follow a similar pattern. However, the core at 2.3 km water depth shows a 0.3‰ decrease in $\delta^{13}C$ during the deglaciation (Figure 4). There is limited evidence for similar excursions at 3.4 km (Figure 5) and 3.6 km (Figure 4) but these $\delta^{13}C$ time series are sparse compared to the shallower core. If $\delta^{18}O$ and $\delta^{13}C$ were decoupled during the last deglaciation, it would suggest that processes in addition to advection and vertical diffusion influenced one or both of the tracers. Deglacial $\delta^{13}C$ anomalies in the North Atlantic have been interpreted to represent the influence of

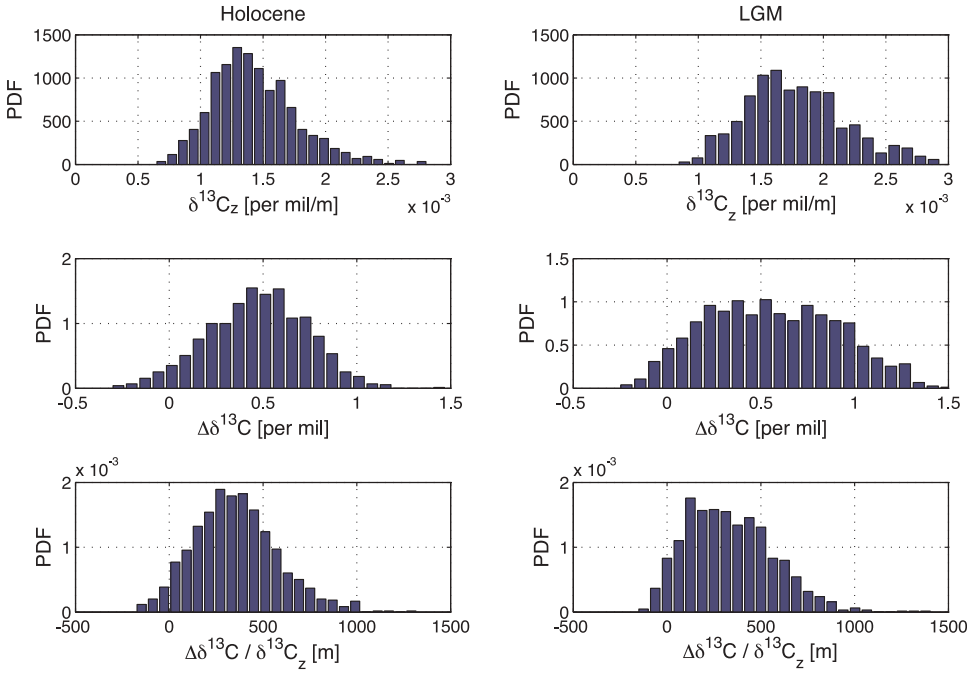

Figure 11. PDFs of $\delta^{13}C_z$, $\Delta\delta^{13}C$, and $\Delta\delta^{13}C/\delta^{13}C_z$ for the (left) Holocene and (right) LGM. Mean values and uncertainties are reported in Tables 2 and 3. The $\Delta\delta^{13}C/\delta^{13}C_z$ distributions are similar for each time interval.

brine water from the Nordic Seas [e.g., *Dokken and Jansen*, 1999; *Meland et al.*, 2008; *Waelbroeck et al.*, 2011] but similar anomalies have not been observed in the Southeast Atlantic [*Waelbroeck et al.*, 2011]. Further study of this issue will require detailed deglacial $\delta^{18}O$ and $\delta^{13}C$ profiles from the Brazil Margin that are constrained with radiocarbon chronologies.

4. Conclusions

[34] Stable isotopic data from the abyssal Southwest Atlantic are key parameters in the tracer budget for AABW. Due to a lack of core material below 3000 m water depth, previous estimates of abyssal $\delta^{18}O$ and $\delta^{13}C$ were based on water column data (for the Holocene) or extrapolation of trends from shallower in the water column (for the LGM) [*Lund et al.*, 2011]. To address these data gaps, we developed several new stable isotope time series from 3 to 4 km water depth at the Brazil Margin. We find that core top $\delta^{18}O$ and $\delta^{13}C$ values at ~4 km water depth are indistinguishable from estimates based on hydrographic data. The core top results from Brazil Margin also yield tracer budget parameters consistent with water column based results spanning the entire Southwest Atlantic. Thus, the spatially limited core top data characterize a broad geographic area, increasing our confidence that the Brazil Margin profile was representative of the Southwest Atlantic during the LGM.

[35] Our LGM $\delta^{18}O$ results at ~4 km water depth are the heaviest values in the published literature and are therefore the best available estimate for AABW as it entered the Southwest Atlantic. Using the new $\delta^{18}O$ data, we estimate that Ψ/K for AABW was about ten times larger than today. Our $\delta^{18}O$ tracer budget results support the preliminary work of *Lund et al.* [2011] that was based on Brazil Margin cores from shallower than 3000 m. In contrast, we find that $\delta^{13}C$ at 4 km water depth was ~0.5‰ more positive than previously assumed. As a result, our estimate of *Pe*, the ratio of tracer transport to tracer diffusion, is lower than the initial estimate of *Lund et al.* [2011] and it now appears that $\delta^{13}C$ acted as a largely conservative tracer during the LGM. Both $\delta^{18}O$ and $\delta^{13}C$ yield similar LGM estimates of Ψ/K, suggesting that either enhanced transport of AABW or reduced mixing across its upper boundary were the primary controls on each tracer profile.

[36] Although $\delta^{13}C$ may have acted conservatively during the LGM and Holocene, some of the cores at the Brazil Margin have a negative excursion in $\delta^{13}C$ during the deglaciation that is not coupled to a simultaneous increase in $\delta^{18}O$. The decoupling of the two tracers suggests that $\delta^{13}C$ may have acted non-conservatively. Further understanding of this issue will require a detailed tracer budget analysis of $\delta^{13}C$ and $\delta^{18}O$ profiles at multiple time slices during the deglaciation.

References

Angulo, R. J., P. J. Reimer, M. C. de Souza, R. Scheel-Ybert, M. C. Tenorio, S. T. Disaro, and M. D. Gaspar (2007), A tentative determination of upwelling influence on the paleosurficial marine water reservoir effect in southeastern Brazil, *Radiocarbon*, *49*(3), 1255–1259.

Clark, P. U., A. S. Dyke, J. D. Shakun, A. E. Carlson, J. Clark, B. Wohlfarth, J. X. Mitrovica, S. W. Hostetler, and A. M. McCabe (2009), The Last Glacial Maximum, *Science*, *325*(5941), 710–714, doi:10.1126/science.1172873.

Curry, W. B., and G. P. Lohmann (1982), Carbon isotopic changes in benthic foraminifera from the western South Atlantic: Reconstruction of glacial abyssal circulation patterns, *Quat. Res.*, *18*(2), 218–235, doi:10.1016/0033-5894(82)90071-0.

Curry, W. B., and D. W. Oppo (2005), Glacial water mass geometry and the distribution of delta C-13 of Sigma CO2 in the western Atlantic Ocean, *Paleoceanography*, *20*, PA1017, doi:10.1029/2004PA001021.

Dokken, T. M., and E. Jansen (1999), Rapid changes in the mechanism of ocean convection during the last glacial period, *Nature*, *401*, 458–461, doi:10.1038/46753.

Duplessy, J. C., N. J. Shackleton, R. G. Fairbanks, L. Labeyrie, D. Oppo, and N. Kallel (1988), Deepwater source variations during the last climatic cycle and their impact on the global deepwater circulation, *Paleoceanography*, *3*(3), 343–360, doi:10.1029/PA003i003p00343.

Hodell, D. A., C. D. Charles, J. H. Curtis, P. G. Mortyn, U. S. Ninnemann, and K. A. Venz (2003), Data Report: Oxygen Isotope Stratigraphy of ODP Leg 177 Sites 1088, 1089, 1090, 1093, and 1094, *Proc. Ocean Drill. Program Sci. Results*, *177*, 26 pp., doi:10.2973/odp.proc.sr.177.120.2003.

Kroopnick, P. M. (1985), The distribution of ^{13}C of ΣCO_2 in the world oceans, *Deep Sea Res., Part A*, *32*(1), 57–84, doi:10.1016/0198-0149(85)90017-2.

Lund, D. C., J. F. Adkins, and R. Ferrari (2011), Abyssal Atlantic circulation during the Last Glacial Maximum: Constraining the ratio between transport and vertical mixing, *Paleoceanography*, *26*, PA1213, doi:10.1029/2010PA001938.

Mackensen, A., H. W. Hubberten, T. Bickert, G. Fischer, and D. K. Fütterer (1993), The $\delta^{13}C$ in benthic foraminiferal tests of *Fontbotia wuellerstorfi* (Schwager) Relative to the $\delta^{13}C$ of dissolved inorganic carbon in Southern Ocean Deep Water: Implications for glacial ocean circulation models, *Paleoceanography*, *8*(5), 587–610, doi:10.1029/93PA01291.

Marchal, O., and W. B. Curry (2008), On the abyssal circulation in the glacial Atlantic, *J. Phys. Oceanogr.*, *38*(9), 2014–2037, doi:10.1175/2008JPO3895.1.

Meland, M. Y., T. M. Dokken, E. Jansen, and K. Hevrøy (2008), Water mass properties and exchange between the Nordic seas and the northern North Atlantic during the period 23–6 ka: Benthic oxygen isotopic evidence, *Paleoceanography*, *23*, PA1210, doi:10.1029/2007PA001416.

Ninnemann, U. S., and C. D. Charles (2002), Changes in the mode of Southern Ocean circulation over the last glacial cycle revealed by foraminiferal stable isotopic variability, *Earth Planet. Sci. Lett.*, *201*(2), 383–396, doi:10.1016/S0012-821X(02)00708-2.

Ostermann, D. R., and W. B. Curry (2000), Calibration of stable isotopic data: An enriched $\delta^{18}O$ standard used for source gas mixing detection and correction, *Paleoceanography*, *15*(3), 353–360, doi:10.1029/1999PA000411.

Sortor, R. N., and D. C. Lund (2011), No evidence for a deglacial intermediate water $\Delta^{14}C$ anomaly in the SW Atlantic, *Earth Planet. Sci. Lett.*, *310*, 65–72, doi:10.1016/j.epsl.2011.07.017.

Speer, K. G., and W. Zenk (1993), The flow of Antarctic Bottom Water into the Brazil Basin, *J. Phys. Oceanogr.*, *23*(12), 2667–2682, doi:10.1175/1520-0485(1993)023<2667:TFOABW>2.0.CO;2.

Waelbroeck, C., L. C. Skinner, L. Labeyrie, J.-C. Duplessy, E. Michel, N. Vazquez Riveiros, J.-M. Gherardi, and F. Dewilde (2011), The timing of deglacial circulation changes in the Atlantic, *Paleoceanography*, *26*, PA3213, doi:10.1029/2010PA002007.

J. L. Hoffman and D. C. Lund, Department of Earth and Environmental Sciences, University of Michigan, 2534 CC Little Bldg., 1100 N. University Ave., Ann Arbor, MI 48109, USA. (dclund@umich.edu)